

# Seismic liquefaction: centrifuge and numerical modeling

P. M. Byrne & S. S. Park

*Department of Civil Engineering, University of British Columbia, BC, Canada*

M. Beaty

*Senior Engineer, Calif. Dept. of Water Resources, Sacramento, CA, USA*

**ABSTRACT:** A fully coupled effective stress dynamic analysis procedure for modeling seismic liquefaction is presented. An elastic plastic formulation is used for the constitutive model UBCSAND in which the yield loci are radial lines of constant stress ratio and the flow rule is non-associated. This is incorporated into the 2D version of FLAC by modifying the existing Mohr-Coulomb model.

This numerical procedure is used to simulate centrifuge test data from the Rensselaer Polytechnic Institute (RPI). UBCSAND is first calibrated to cyclic simple shear tests performed on Nevada sand. Both pre- and post-liquefaction behaviour is captured. The centrifuge tests are then modeled and the predicted accelerations, excess porewater pressures, and displacements are compared with the measurements. The results are shown to be in general agreement when stress densification and saturation effects are taken into account.

The procedure is currently being used in the design of liquefaction remediation measures for a number of dam, bridge, tunnel, and pipeline projects in Western Canada.

## 1 INTRODUCTION

Displacements arising from seismic liquefaction can be very large and are a major concern for earth structures located in regions of moderate to high seismicity. Liquefaction is caused by high porewater pressures resulting from the tendency for granular soils to compact when subjected to cyclic loading. Remedial measures typically involve attempts to prevent or curtail liquefaction so that displacements are reduced to tolerable levels. Modifications can also be made to the structure so that larger displacements can be tolerated. In either case, the rational design for remediation requires a reliable prediction of soil-structure response during the design earthquake.

State-of-practice procedures for evaluating liquefaction typically use separate analyses for liquefaction triggering (e.g. Youd et al. 2001), flow slide (limit equilibrium with residual strength), and displacements (Newmark sliding block). While the results of the triggering evaluation are used as input into the flow slide and displacement evaluations, the analyses are otherwise independent. While this practice often provides a good screening level tool, these simplified total stress analyses cannot reliably predict excess porewater pressures, accelerations, or displacement patterns.

State-of-art procedures involve dynamic finite element or finite difference analyses using effective

stress procedures coupled with fluid flow predictions. These analyses can estimate the displacements, accelerations and porewater pressures caused by a specified input motion. Triggering of liquefaction, displacements and flow slide potential are addressed in a single analysis. Such analyses involve capturing the liquefaction behaviour of a soil element as observed in laboratory tests, and then modeling the soil-structure as a collection of such elements subjected to the design earthquake base motion.

It is vital that these sophisticated procedures be verified before they are used in practice. Instrumented centrifuge model tests can be used for verification and have some advantages over observed field behaviour. Centrifuge tests allow the measurement of displacements, input and induced accelerations, and porewater pressures under field stress conditions. These tests can therefore provide a useful database for verification of numerical modeling. This approach is used below.

## 2 LIQUEFACTION

Liquefaction is caused by the tendency of granular soil to contract when subjected to monotonic or cyclic shear loading. When this contraction is prevented or curtailed by the presence of water in the pores, normal stress is transferred from the soil

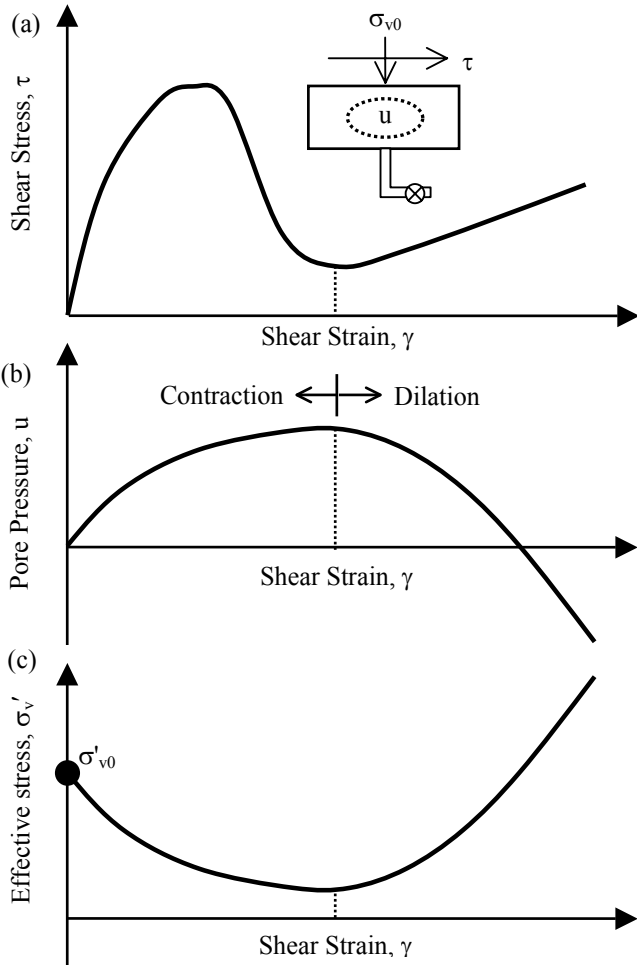


Figure 1. Undrained response of loose sand in simple shear: (a) stress-strain, (b) pore pressure, and (c) effective stress response.

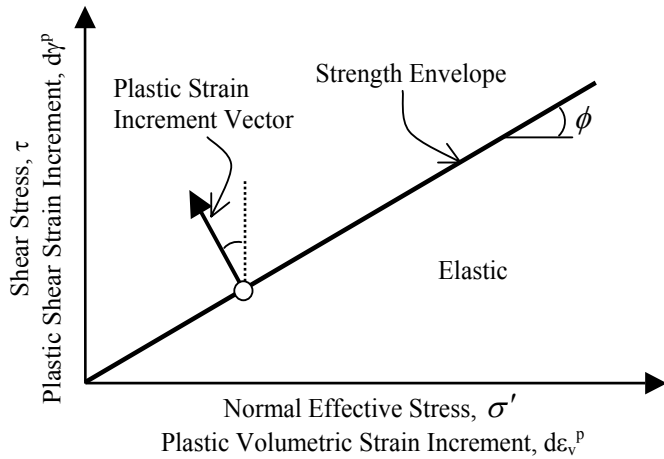


Figure 2. Classic Mohr-Coulomb model.

skeleton to the water. This can cause high excess pore pressures resulting in a very large reduction in shear stiffness. Large shear strains may occur, and the soil will dilate with these strains unless the soil is very loose. This dilation causes the porewater pressure to drop and the stiffness to increase which can

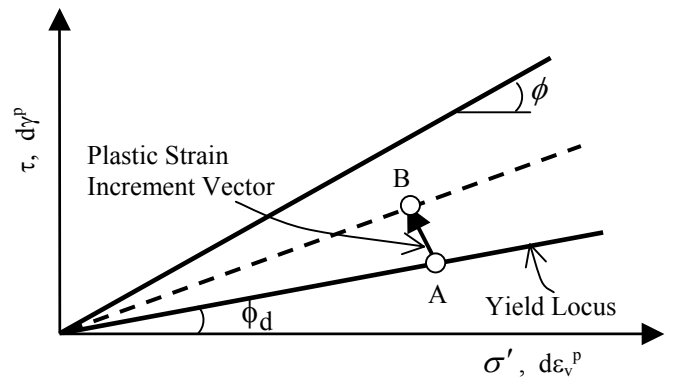


Figure 3. UBCSAND model.

limit the strains induced by a load cycle. This behaviour is illustrated in Figure 1 for monotonic loading.

It is this tendency of the soil skeleton to contract and dilate that controls its liquefaction response. Once the skeleton behaviour is modeled, the response under drained, undrained or coupled stress-flow conditions can be computed by incorporating the bulk stiffness and flow of the pore fluid.

### 3 CONSTITUTIVE MODEL: UBCSAND

The simplest realistic model for soil is the classic Mohr-Coulomb elastic-plastic model as depicted in Figure 2. Soils are modeled as elastic below the strength envelope and plastic on the strength envelope with plastic shear and volumetric strains increments related by the dilation angle,  $\psi$ . This model is really too simple for soils since plastic strains also occur for stress states below the strength envelope. The UBCSAND stress-strain model described herein modifies the Mohr-Coulomb model incorporated in FLAC to capture the plastic strains that occur at all stages of loading. Yield loci are assumed to be radial line of constant stress ratio as shown in Figure 3. Unloading is assumed to be elastic. Reloading induces plastic response but with a stiffened plastic shear modulus.

The plastic shear modulus relates the shear stress and the plastic shear strain and is assumed to be hyperbolic with stress ratio as shown in Figure 4. Moving the yield locus from A to B in Figure 3 requires a plastic shear strain increment,  $\Delta\gamma^P$ , as shown in Figure 4, and is controlled by the plastic shear modulus,  $G^P$ . The associated plastic volumetric strain increment,  $d\varepsilon_v^P$ , is obtained from the dilation angle  $\psi$ :

$$\Delta\varepsilon_v^P = \Delta\gamma^P \cdot \sin \psi \quad (1)$$

The dilation angle is based on laboratory data and energy considerations and is approximated by

$$\sin \psi = \sin \phi_d - \sin \phi_{cv} \quad (2)$$

where  $\phi_{cv}$  is the phase transformation or constant volume friction angle and  $\phi_d$  describes the current

yield locus. A negative value of  $\psi$  corresponds to contraction. Contraction occurs for stress states below  $\phi_{cv}$  and dilation above as shown in Figure 5.

Additional information on earlier but similar forms of UBCSAND is presented by Puebla et al. (1997) and Beaty & Byrne (1998).

Elastic and plastic properties for the model are defined as follows.

### 3.1 Elastic Properties

The elastic bulk modulus,  $B$ , and shear modulus,  $G^e$ , are assumed to be isotropic and stress level dependent. They are described by the following relations where  $k_B$  and  $k_G$  are modulus numbers,  $P_A$  is atmospheric pressure, and  $\sigma'_m$  is the mean effective stress:

$$B = k_B \cdot P_A \cdot \left( \frac{\sigma'_m}{P_A} \right)^{0.5} \quad (3)$$

$$G^e = k_G \cdot P_A \cdot \left( \frac{\sigma'_m}{P_A} \right)^{0.5} \quad (4)$$

### 3.2 Plastic Properties

The plastic properties used by the model are the peak friction angle  $\phi_p$ , the constant volume friction angle  $\phi_{cv}$ , and plastic shear modulus  $G^P$ , where

$$G^P = G_i^P \cdot \left( 1 - \frac{\tau}{\tau_f} R_f \right)^{0.5} \quad (5)$$

$G_i^P = \alpha G^e$  and  $\alpha$  depends on relative density,  $\tau$  is the current shear stress,  $\tau_f$  is the projected shear stress at failure, and  $R_f$  is the failure ratio used to truncate the hyperbolic relationship.

The position of the yield locus  $\phi_d$  is known for each element at the start of each time step. If the stress ratio increases and plastic strain is predicted, then the yield locus for that element is pushed up by an amount  $\Delta\phi_d$  as given by Equation 6. Unloading of stress ratio is considered to be elastic. Upon reloading, the yield locus is set to the stress ratio corresponding to the stress reversal point.

$$\Delta\phi_d = \left( \frac{G^P}{\sigma'_m} \right) \cdot \Delta\gamma^P \quad (6)$$

The elastic and plastic parameters are highly dependent on relative density, which must be considered in any model calibration. These parameters can be selected by calibration to laboratory test data. The response of the model can also be compared to a considerable database for triggering of liquefaction under earthquake loading in the field. This database exists in terms of penetration resistance, typically from cone penetration (CPT) or standard penetration (SPT) tests. A common relationship between  $(N_1)_{60}$  values from the SPT and the cyclic stress ratio that triggers liquefaction for a magnitude 7.5 earthquake

is given by Youd et al. (2001). Comparing laboratory data based on relative density to field data based on penetration resistance relies upon an approximate conversion, such as that proposed by Skempton (1986):

$$35 < \frac{(N_1)_{60}}{D_r^2} < 60 \quad (7)$$

Model parameters based on penetration resistance and field observation may be useful for field conditions where it is very difficult to retrieve and test a representative sample. However, this indirect method is not appropriate for simulation of centrifuge models. Calibrations for this case should be based on direct laboratory testing of samples that are prepared in the same manner as the centrifuge model.

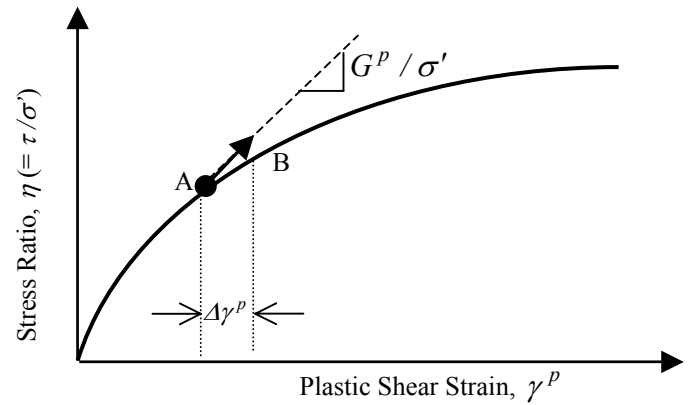


Figure 4. Hyperbolic stress-strain relationship.

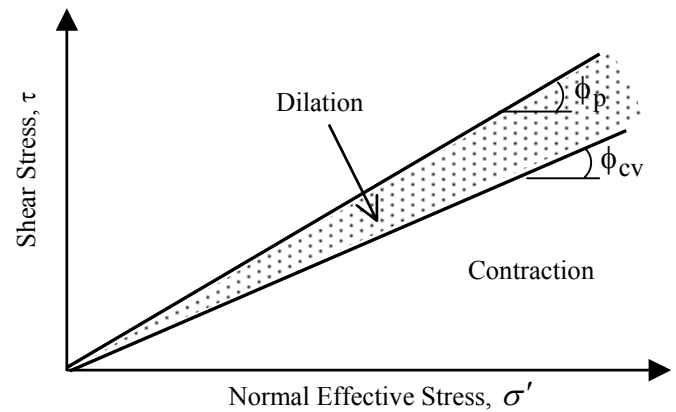


Figure 5. Zones of shear-induced contraction and dilation.

## 4 SIMULATION OF CYCLIC ELEMENT TEST DATA

A number of cyclic simple shear tests have been conducted on Fraser River sand at the University of British Columbia. The samples were prepared by air pluviation with a target relative density  $D_r$  of 40%

and tested at an initial vertical effective stress,  $\sigma'_{vo}$ , of 100 kPa. Samples were also tested at  $\sigma'_{vo}$  of 200 kPa with a  $D_r$  of 44%. Samples were subjected to cyclic shear under constant volume conditions that simulate undrained response at a range of cyclic stress ratios. Typical examples of measured response are shown in Figures 6 and 7. From Figure 6a it may be seen that as the shear stress is cycled, the effective stresses decrease as the pore pressure ratio  $r_u$  increases. This ratio  $r_u$  is given by  $(u - u_0) / \sigma'_{vo}$ , where  $u_0$  and  $u$  are the initial and current pore pressures.  $r_u$  approaches unity after 5 cycles, which corresponds to a state of zero effective stress. Application of further cycles produce very large shear strains in the range of 10 to 15% or more as shown in Figure 6b. However, the strain per cycle is limited as the pore pressures drop with strain due to dilation.

Figures 6 and 7 also show the response predicted using UBCSAND. The elastic and plastic parameters selected by the calibration were the same for both tests. The model gives a reasonable representation of the observed response, although the final predicted strains are less than measured for Figure 6. A summary of the test results and the UBCSAND calibration are shown in Figure 8. The predicted and measured liquefaction response for  $\sigma'_{vo}$  of 100 and 200 kPa is in close agreement.

## 5 CENTRIFUGE TESTS

A simulation using UBCSAND was made of 2 centrifuge tests carried out at RPI as described in Table 1. In the centrifuge test, a small model is used that is subjected to a high acceleration field during the test. This has the effect of increasing its stresses by the ratio of the induced acceleration divided by the acceleration of gravity. This ratio or factor is 120 for Model 1 and 60 for Model 2 as indicated by Table 1. The centrifuge model under the increased acceleration field can also be thought of as representing a prototype that is 120 (Model 1) or 60 (Model 2) times larger than the actual model. Results from the centrifuge test can be presented at either the model or prototype scale. The prototype scale is used for this paper.

While in flight, a motion simulating an earthquake time history is applied to the base of the model. For dynamic similitude at the model scale, the earthquake time scale must be decreased by a factor of 120 (Model 1) or 60 (Model 2), and the earthquake acceleration increased by the same factor. The engineering coefficient of permeability  $k$  will also increase by this same factor due to the increased unit weight of the fluid.  $k$  should be decreased for hydraulic similitude, although it is not necessary to model a specific  $k$ . It is common to use a fluid in the test that is 30 to 60 times more viscous than water to

prevent rapid rates of dissipation that might unduly curtail liquefaction effects.

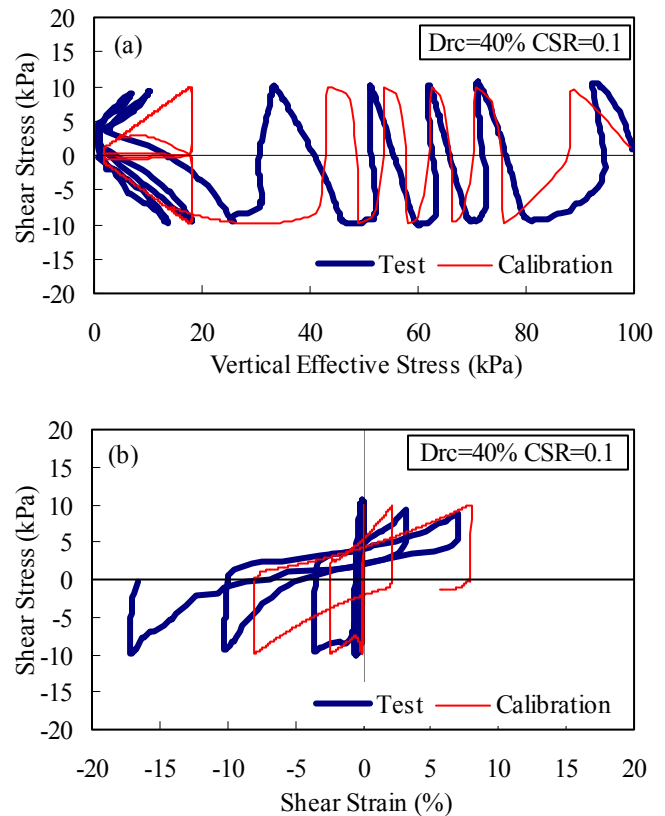


Figure 6. Stress path and stress-strain relationship ( $CSR=0.1$ ).

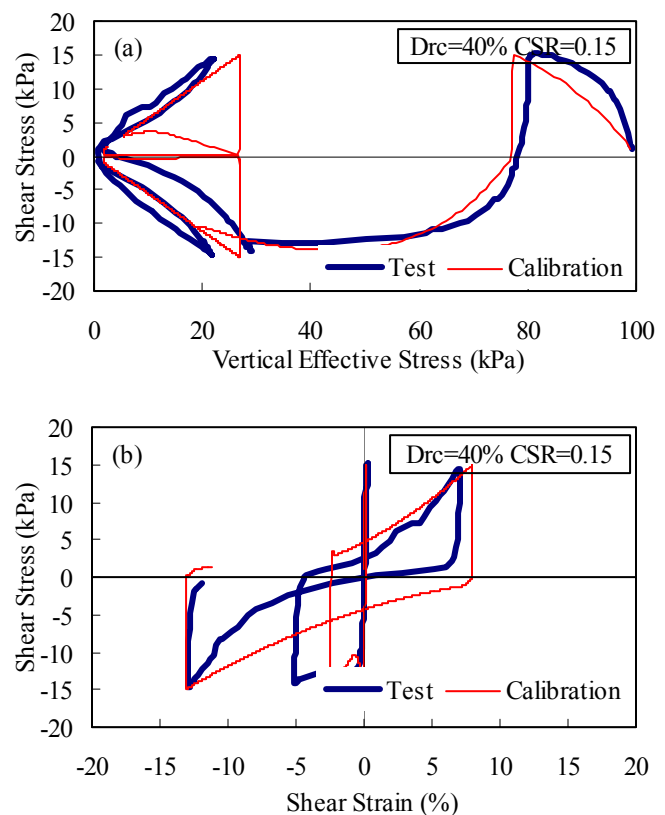


Figure 7. Stress path and stress-strain relationship ( $CSR=0.15$ ).

Nevada sand was used for these centrifuge tests and its liquefaction and permeability (at 1g using water as pore fluid) properties were obtained from laboratory tests (Arulmoli et al. 1992, Kammerer et al. 2000, Taboada-Urtuzuastegui et al. 2002). Its measured liquefaction resistance together with the UBCSAND prediction is shown in Figure 9.

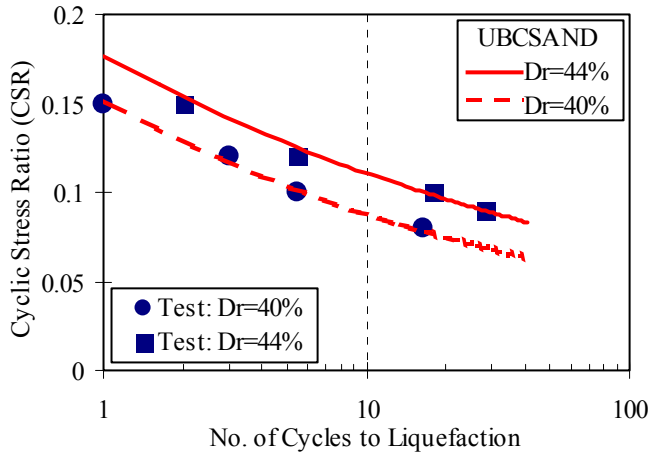


Figure 8. Predicted and measured liquefaction response of Fraser River sand.

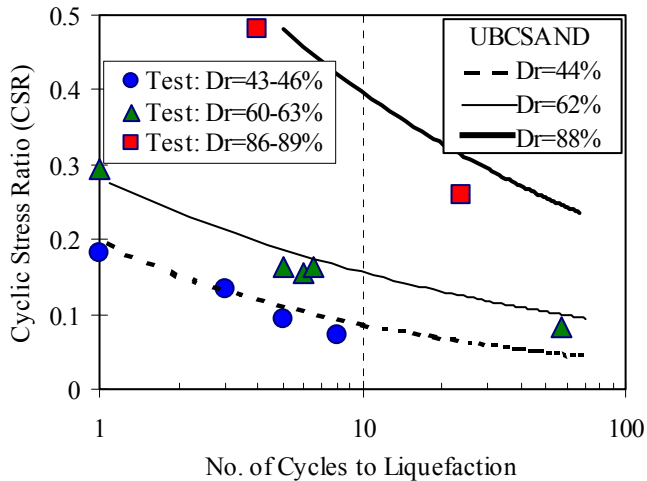


Figure 9. Liquefaction resistance of Nevada sand.

Table 1. Centrifuge model tests.

	RPI Model 1	RPI Model 2
Test condition	Level	Slope
$D_r$	55 %	40 %
Centrifuge Acc.	120 g	60 g
Max. $\sigma'_v$	380 kPa	100 kPa
Soil depth	38 m	10 m
Fluid viscosity	60 $\mu\text{w}$	60 $\mu\text{w}$

## 5.1 Model 1

Model 1 comprises a uniform horizontal sand layer having a thickness of 37 m (prototype scale) and a placement density  $D_r$  of 55% as shown in Figure 10 (Gonzalez et al. 2002). After application of the 120 g acceleration field,  $D_r$  was estimated to increase to 63% near the base due to the increase in stresses. The amount of densification was estimated from one-dimensional compression tests. The applied base motion is shown in Figure 11 and consisted of 50 cycles with an amplitude of 0.2 g and a frequency of 1.5 Hz. The key inputs including water bulk stiffness ( $B_f$ ) for different layers in the numerical model are listed in Table 2.

The container for Model 1 consisted of slip “rings” that allowed differential horizontal displacements in the vertical direction but not in the horizontal. This was simulated in the FLAC model by “attaching” the vertical sides, Figure 10. The initial horizontal effective stresses were set to 0.5 times the vertical effective stresses.

The measured and predicted excess pore pressures and accelerations for various depths are shown in Figure 12. The predicted accelerations are initially about the same at all depths and approximately equal to the base input value of 0.2 g. The accelerations decrease over much of the model as the shaking continues. The decay of acceleration is most rapid in the upper layers and can be explained in terms of the excess porewater pressures shown in Figure 12b. A large drop in acceleration response occurs when the measured excess pore pressure reaches the initial vertical effective stress  $\sigma'_{v0}$  which corresponds to a liquefied state. Measurements show that liquefaction occurs first near the surface and then progresses downward. The accelerations and excess pore pressures predicted using UBCSAND are in generally good agreement with the measurements.

The analysis described above incorporates the effect of densification due to the increased acceleration field. If this effect is not considered, and a uniform  $D_r$  of 55% is used in the analysis, then liquefaction is predicted to occur first at the base of the model rather than at the surface. The higher  $D_r$  at the base reverses this trend and indicates the importance of stress densification in centrifuge tests.

Full saturation of the pores is difficult to achieve in a centrifuge test. The best fit with the data was obtained assuming an initial placement saturation, or  $S_r$ , of 98% at atmospheric pressure. The pore pressure will increase as the centrifuge acceleration is applied, and the resulting increase in  $S_r$  is modeled using the gas laws.

In summary,

- UBCSAND provides a reasonable agreement to the test results,
- $r_u = 1.0$  and liquefaction can occur at depths of 40 m in medium dense sand strata,

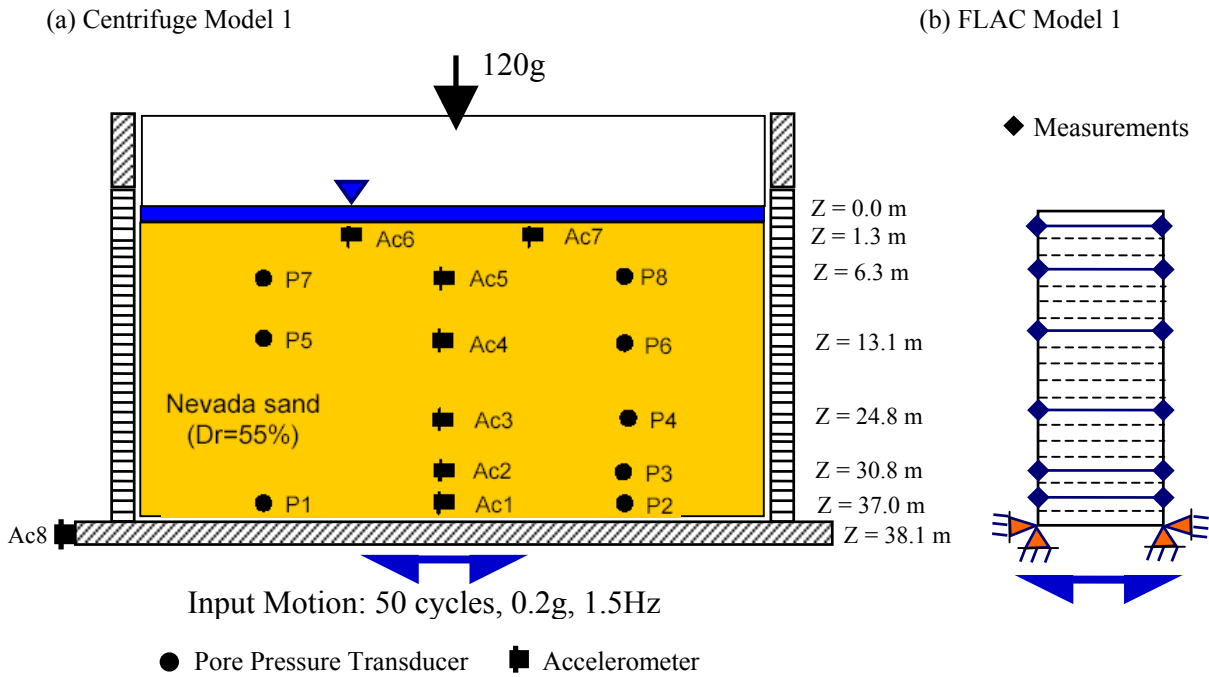


Figure 10. Centrifuge Model 1 and FLAC Model 1.

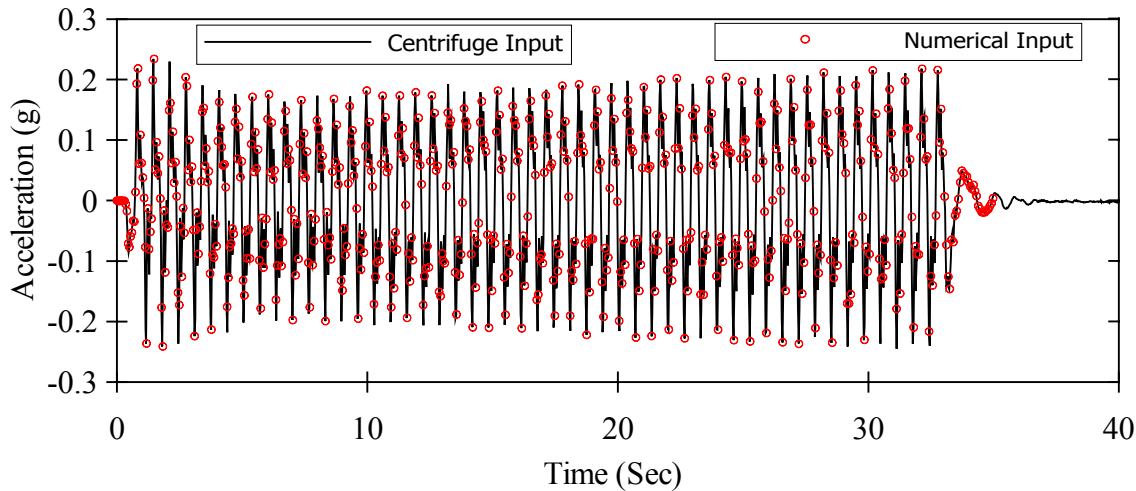


Figure 11. Based input motions of Model 1.

Table 2. Key input for Model 1 numerical analysis.

Layer	$k_G$	$k_B$	$\alpha$	$B_f$ after Spinup	Permeability
				kPa	m/sec
Top	952	2856	0.44	0.2 E5	5 E-5
Middle	1020	3060	0.61	0.6 E5	5 E-5
Bottom	1042	3126	0.67	1.2 E5	5 E-5

- (c) a large reduction in the accelerations can occur upon liquefaction,
- (d) the effect of stress densification should be included, and
- (e) the degree of saturation,  $S_r$ , must be considered.

### 5.2 Model 2

The cross section for Model 2 is shown in Figure 13 and comprises a steep 1.5:1 slope in loose fine sand with  $D_r = 40\%$  (Taboada-Urtuzuastegui et al. 2002). The base motion consists of 20 cycles of 0.2 g at a frequency of 1 Hz. The container for model 2 was rigid and this was simulated in the FLAC model by applying the input motion to the vertical sides as well as the base. The key inputs for Model 2 are listed in Table 3. Pore pressures and accelerations were measured away from the face of the slope, approximating free field conditions, as well as adjacent to the slope.

The predicted and observed accelerations and pore pressures in the free field are shown in Figures 14 and 15. As expected, similar trends are seen as for the level ground test of Model 1, i.e.  $r_u$  of 100% and reduced accelerations.

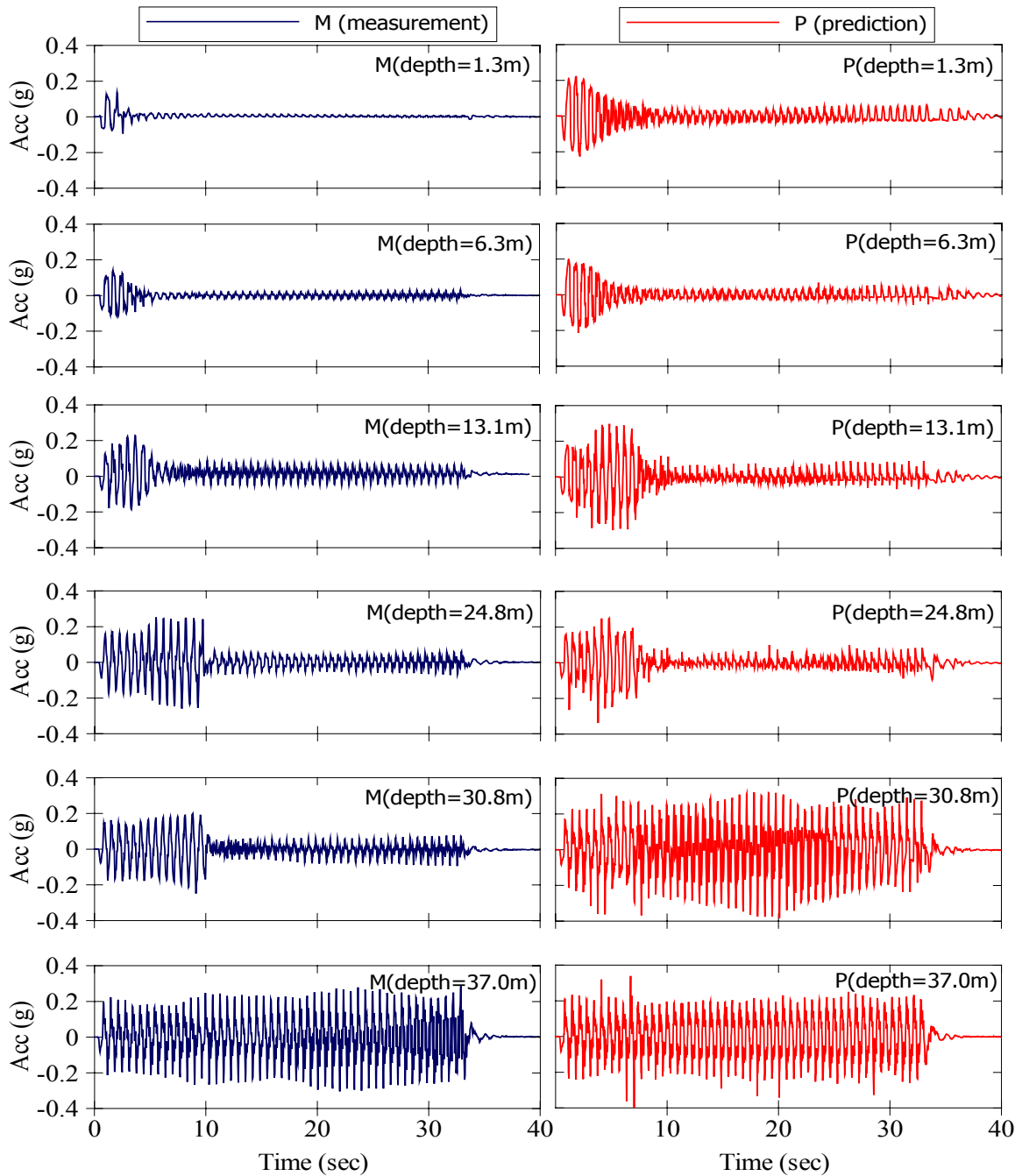


Figure 12a. Measured (left) and predicted (right) accelerations of Model 1.

The accelerations and pore pressures near the slope are shown in Figures 16 and 17. It may be seen in Figure 16 that there is little or no reduction in the accelerations. Instead, large upslope acceleration spikes occur. Excess pore pressures are shown in Figure 17. Large negative excess pore pressure spikes occur that coincide in time with the upslope acceleration spikes. The slope is steep and the upslope acceleration of the base tends to induce failure of the slope and relative downslope movement. The soil dilates as it shears in the downslope direction, producing negative pore pressures which stiffen the shear modulus. Enough strength is mobilized through this dilation to arrest the downslope movement and gives rise to the acceleration spike (Taboada-Urtuzuastegui et al. 2002).

UBCSAND provides a reasonable prediction of the accelerations and pore pressure response for the free field. More significant differences are observed for locations near the slope. Some of these differences are due to UBCSAND under predicting the dilative spikes. This requires further investigation. The measured and predicted displacements after shaking are shown in Figures 18 and 19. It may be seen that both the magnitude and pattern of displacements are in general agreement.

In summary,

- (a) UBCSAND provides reasonable agreement with this centrifuge test, although further study is needed for locations close to the sloping face,
- (b) a decrease in accelerations after liquefaction was not observed near the slope,

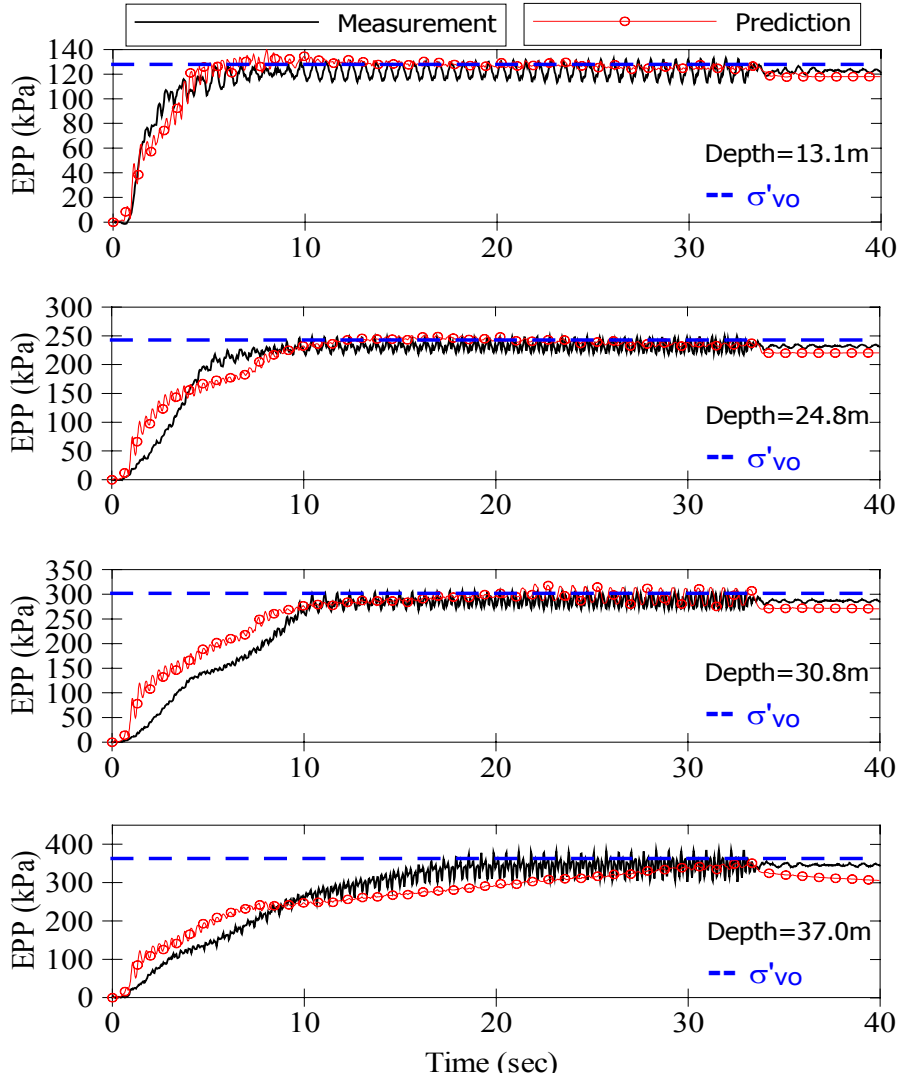


Figure 12b. Measured and predicted excess pore pressures of Model 1.

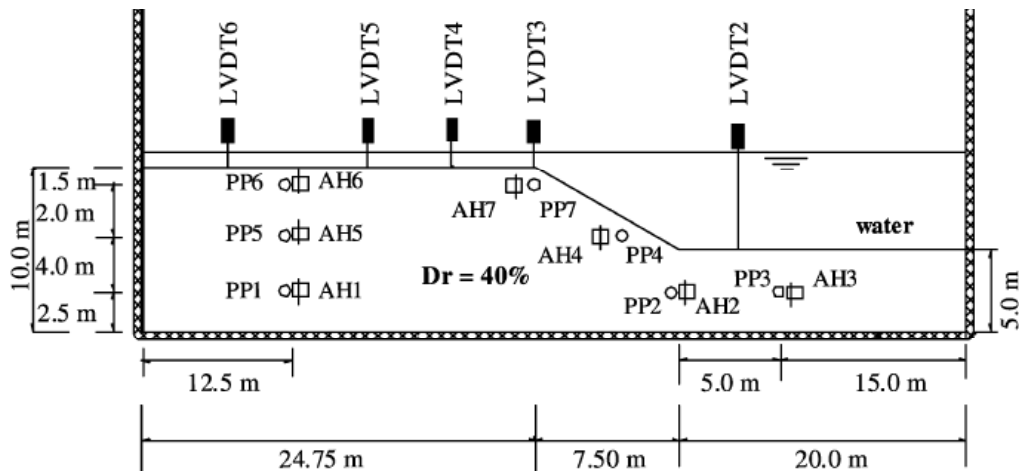


Figure 13. Cross section of Model 2 (Taboada-Urtuzuastegui et al. 2002).

Table 3. Key input for Model 2 numerical analysis.

Layer	$k_G$	$k_B$	$\alpha$	$B_f$ after Spinup	Permeability
				kPa	m/sec
Free field	867	2601	0.22	1.0 E5	2.1 E-5

- (c) a large upslope acceleration spikes occurred near the slope,
- (d) a decrease in pore pressure due to dilation corresponded with these upslope acceleration spikes, and,
- (e) the dilative spikes prevented very large displacements from occurring in this homogeneous fine sand model.

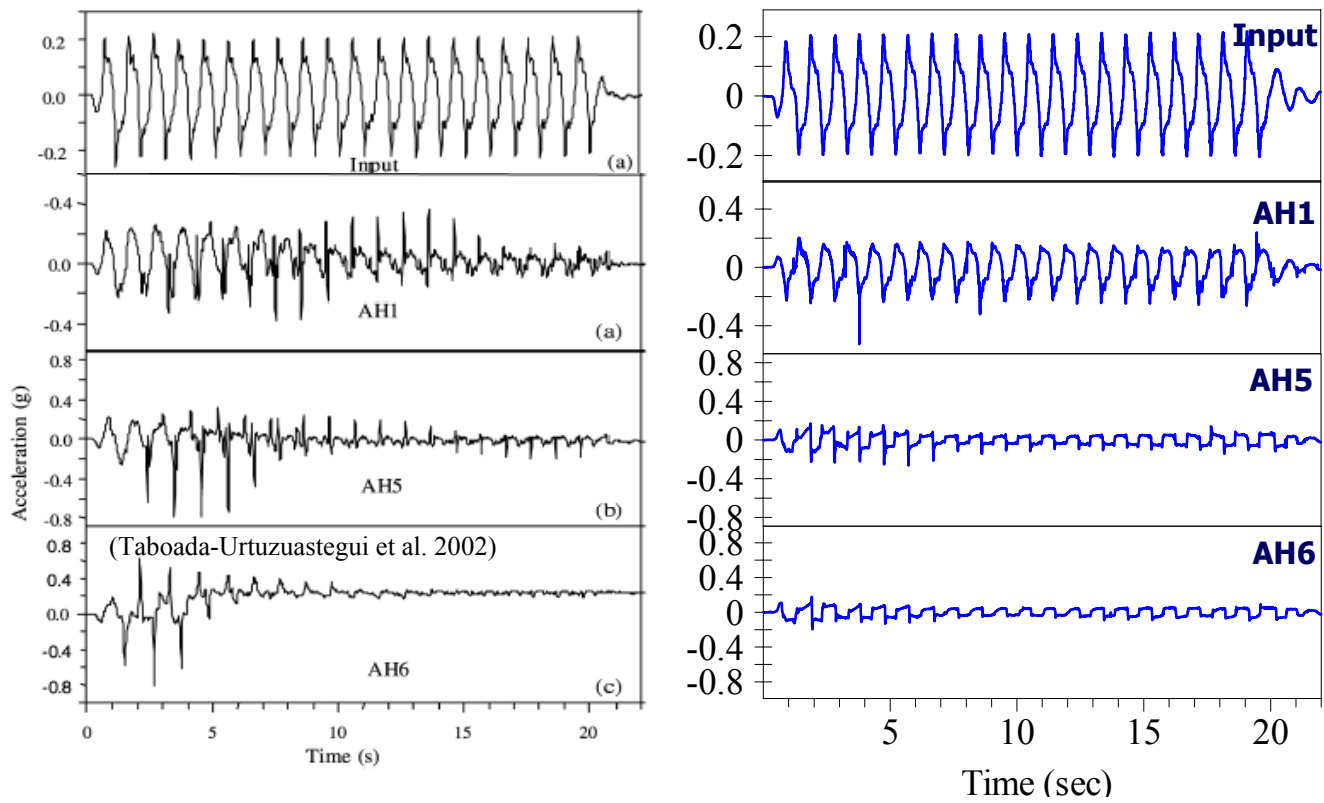


Figure 14. Measured (left) and predicted (right) accelerations at free field.

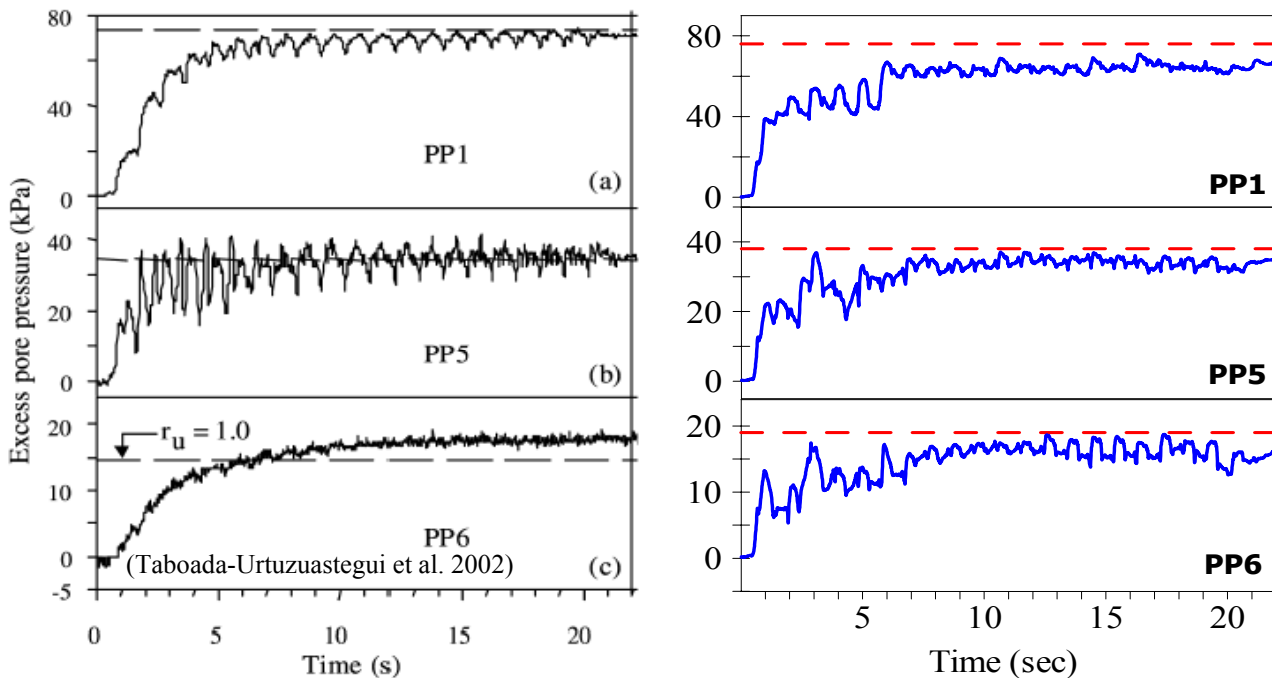


Figure 15. Measured (left) and predicted (right) excess pore pressures at free field.

## 6 SUMMARY

A fully coupled effective stress dynamic analysis procedure has been presented. The procedure is first calibrated by comparison with laboratory element test data and then verified by comparison with two centrifuge model tests.

Model 1 represented a deep sand layer with a level ground condition. This model showed that high excess porewater pressure and liquefaction can occur to depths of 40 m in medium dense sands. Liquefaction first occurred at the surface and progressed downward under continued shaking. Accelerations above the depth of liquefaction showed a significant decrease. The numerical model results were in good agreement with the

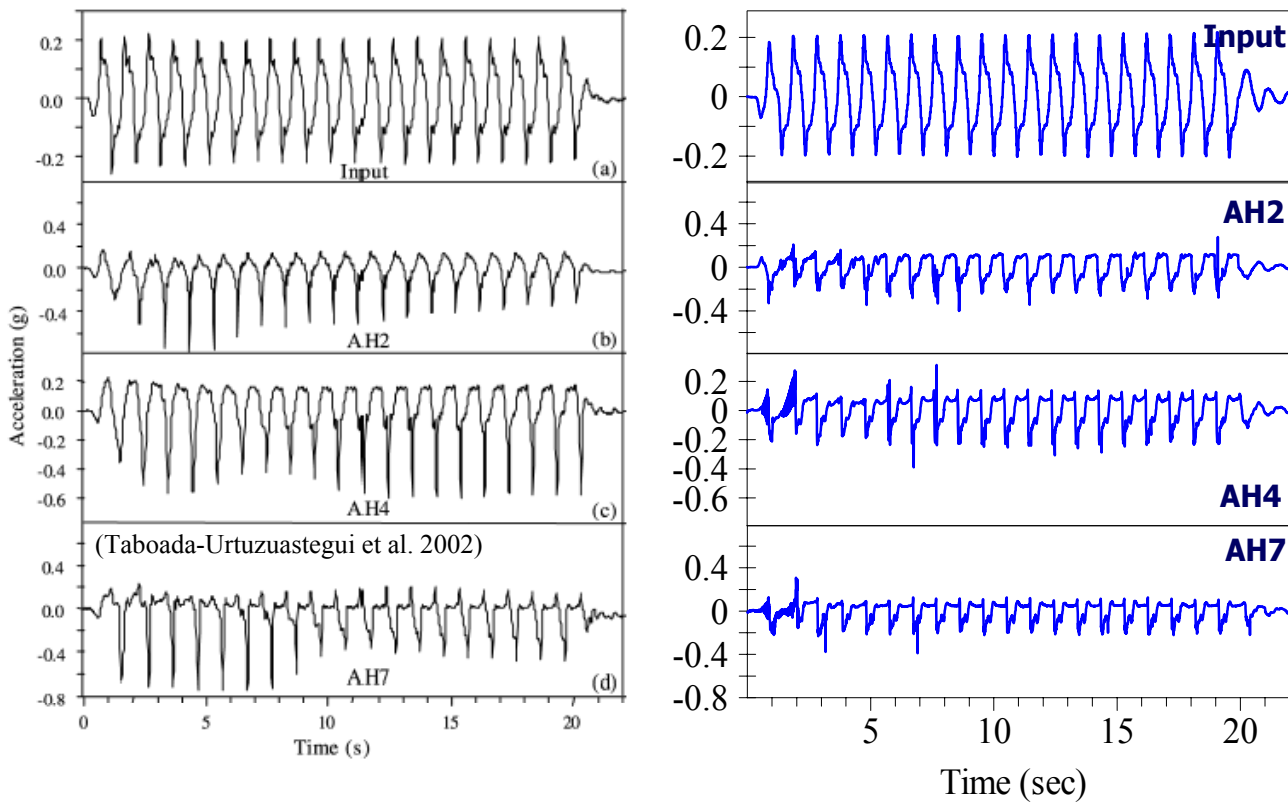


Figure 16. Measured (left) and predicted (right) accelerations near the slope.

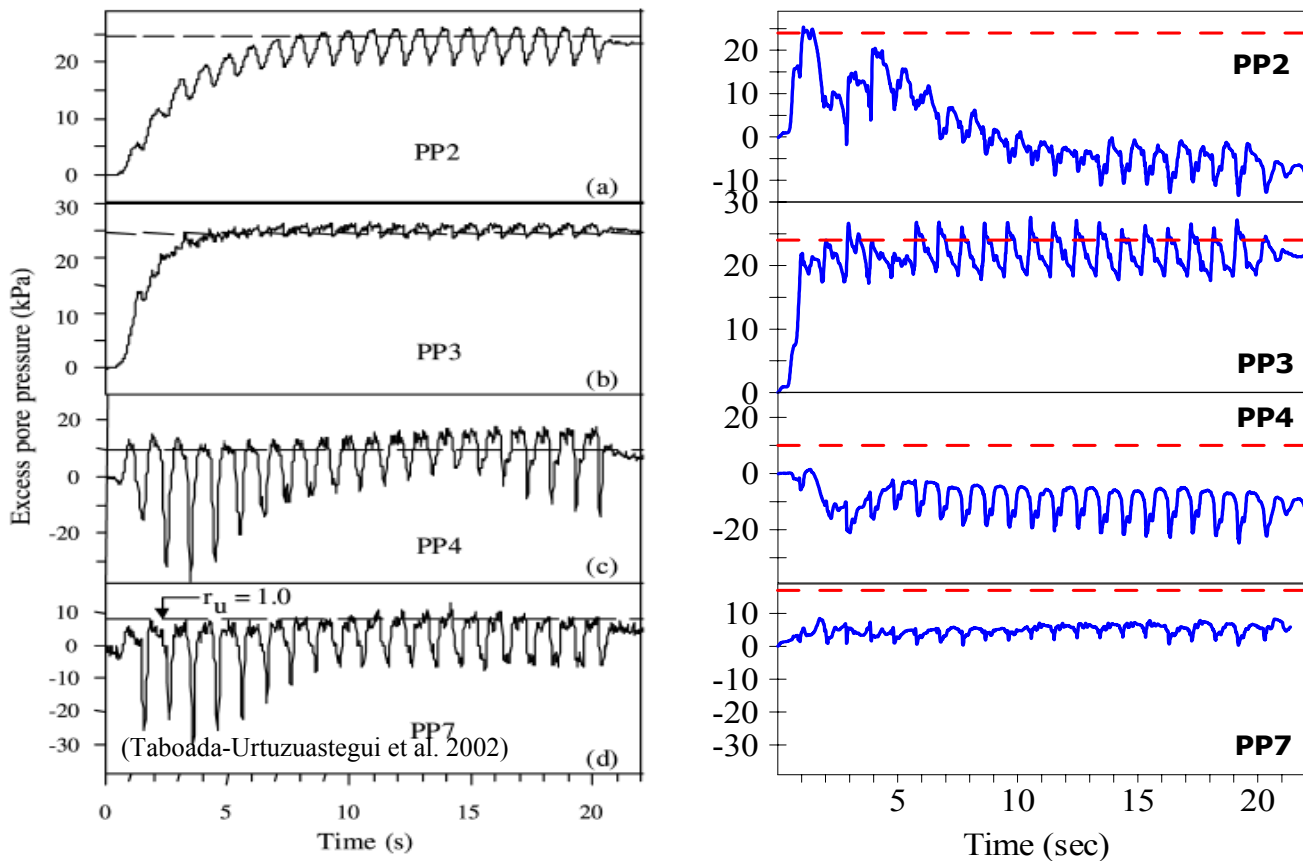


Figure 17. Measured (left) and predicted (right) excess pore pressures near the slope.

measurement when stress densification and saturation effects were included.

Model 2 represented a steep slope condition in homogeneous loose fine sand. The results showed that large upslope acceleration spikes occurred

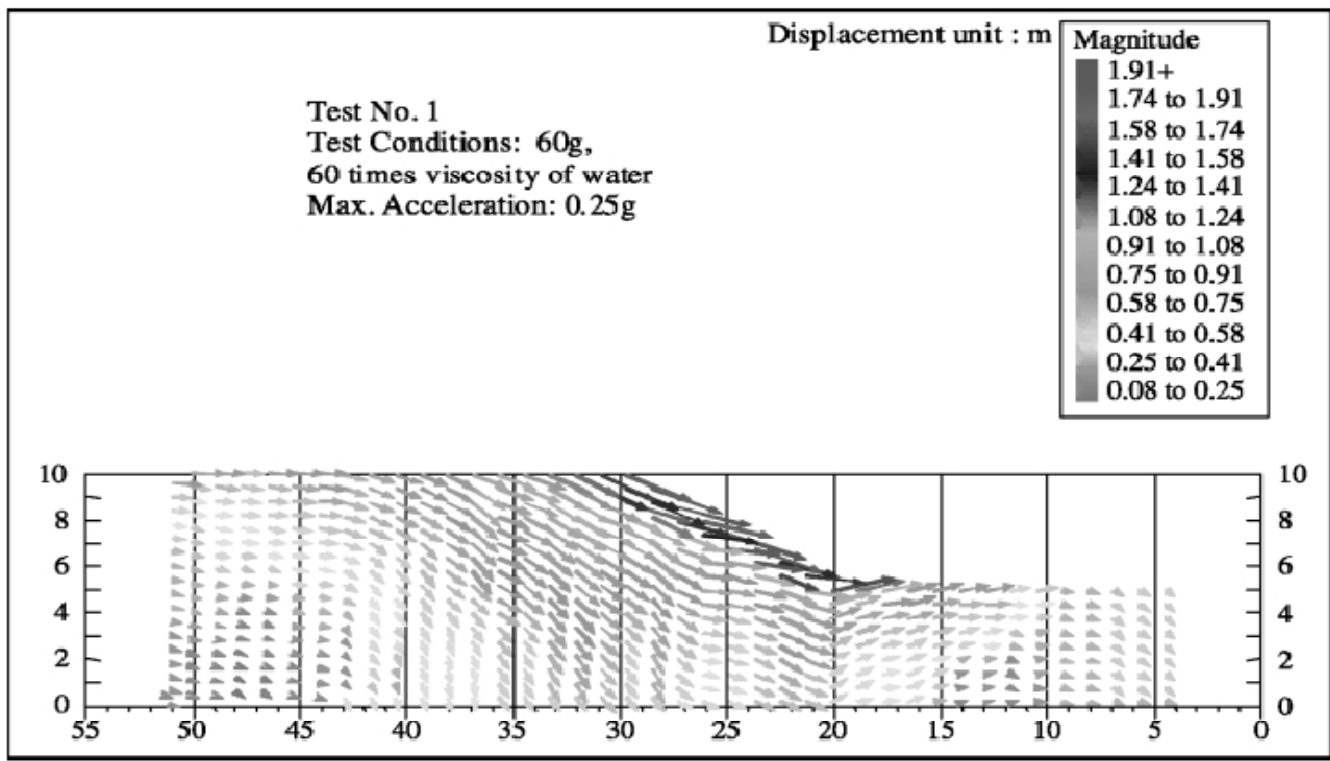


Figure 18. Measured displacements for Model 2 from centrifuge test (Taboada-Urtuzuastegui et al. 2002).

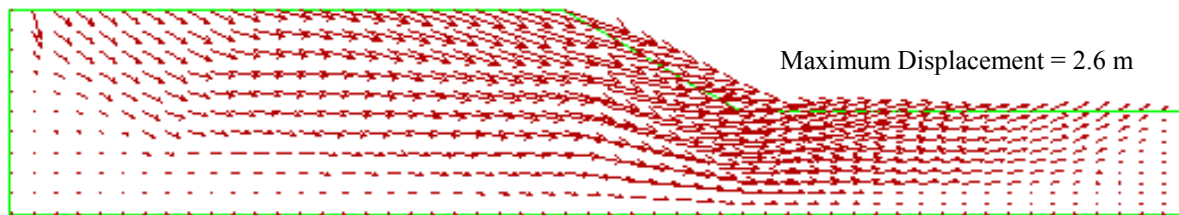


Figure 19. Predicted displacements for Model 2 using UBCSAND.

near the face of the slope after liquefaction. These acceleration spikes corresponded with large negative excess pore pressure spikes associated with dilation. It is the increase in effective stress associated with these negative pore pressure spikes that curtails the displacements and makes the slope more stable than might be expected under cyclic loading. The overall pattern of predicted response is in reasonable agreement with the measurements, although both the acceleration and pore pressure spikes are under predicted by the UBCSAND analysis.

A new series of centrifuge tests are planned at CCORE (Centre for Cold Ocean Research), Memorial University, Newfoundland, which will permit further verification and refinement of the numerical model.

## REFERENCES

Arulmoli, K., Muraleetharan, K.K., Hossain, M.M. & Fruth, L.S. 1992. VELACS laboratory testing program, soil data

report. The Earth Technology Corporation, Irvine, California, Report to the National Science Foundation, Washington D.C., March. Beaty, M. & Byrne, P. 1998. An effective stress model for predicting liquefaction behaviour of sand. ASCE Geot. Special Pub. No. 75: 766-777.

Gonzalez, L, Abdoun, T., & Sharp, M.K. 2002. Modeling of seismically induced liquefaction under high confining stress.

Kammerer, A., Wu, J., Pestana, J., Riemer, M., & Seed, R. 2000. Cyclic simple shear testing of Nevada sand for PEER Center project 2051999. Geotechnical Engineering Research Report No. UCB/GT/00-01, University of California, Berkeley, January.

Puebla, H., Byrne, P.M. & Phillips, R. 1997. Analysis of CANLEX liquefaction embankments: prototype and centrifuge models. Can. Geotech. Journal, Vol. 34, No. 5: 641-657.

Skempton, A.W. 1986. Standard penetration test procedures and the effects in sands of overburden pressure, relative density, particle size, ageing and overconsolidation, Geotechnique 36, No. 3: 425-447.

Taboada-Urtuzuastegui, V.M., Martinez-Ramirez, G. & Abdoun, T. 2002. Centrifuge modeling of seismic behavior of a slope in liquefiable soil, Soil Dynamic and Earthquake Engineering, Vol. 22: 1043-1049.

Youd, T.L., Idriss, I. M., Andrus, R.D., Arango, I., Castro, G., Christian, J.T., Dobry, R., Finn, W.D.L., Harder Jr., L.F., Hynes, M.E., Ishihara, K., Koester, J.P., Liao, S., Marcuson III, W.F., Martin, G.R., Mitchell, J.K., Moriwaki, Y., Power, M.S., Robertson, P.K., Seed, R.B. & Stokoe, K.H. 2001. Liquefaction Resistance of Soils: Summary Report from the 1996 NCEER and 1998 NCEER/NSF Workshops on Evaluation of Liquefaction Resistance of Soils. ASCE J. of Geot. and Geoenv. Eng., Vol. 127, No. 10: 817-833.